Article

Not peer-reviewed version

Beyond the Tide: A Comprehensive Guide to Sea Level Rise Inundation Mapping using FOSS4G

Levente Juhász *, Jinwen Xu, Randall W. Parkinson

Posted Date: 8 November 2023

doi: 10.20944/preprints202311.0504.v1

Keywords: sea level rise; flood; climate change; coastal mapping; inundation mapping; FOSS4G

Article

Beyond the Tide: A Comprehensive Guide to Sea Level Rise Inundation Mapping Using FOSS4G

Levente Juhász [1,*], Jinwen Xu [1] and Randall W. Parkinson [2]

[1] GIS Center, Florida International University, Miami, FL 33199, USA; jinwxu@fiu.edu
[2] Institute of Environment, Florida International University, Miami, FL 33199, USA; rparkins@fiu.edu
* Correspondence: ljuhasz@fiu.edu; Tel.: +1-305-348-6444

Abstract: Sea level rise (SLR) is a critical consequence of climate change, posing significant threats to coastal regions worldwide. Accurate and efficient assessment of potential inundation areas is crucial for effective coastal planning and adaptation strategies. This study aims to explore the utility of free and open source software for geospatial (FOSS4G) tools for mapping SLR inundation, providing cost-effective solutions that are accessible to researchers and policymakers. We employed a combination of geospatial data, including high-resolution elevation models, tidal data, and projected SLR scenarios. Utilizing widely available FOSS4G tools like QGIS, GDAL/OGR and GRASS GIS we developed an integrated workflow to map inundation extents using a passive bathtub approach for various SLR scenarios. Our findings demonstrate that FOSS4G tools offer reliable and accessible means to map SLR inundation, empowering stakeholders to assess coastal vulnerabilities and devise sustainable adaptation measures. The open-source approach facilitates collaboration and reproducibility, fostering a comprehensive understanding of the potential impacts of SLR on coastal ecosystems and communities.

Keywords: sea level rise; flood; climate change; coastal mapping; inundation mapping; FOSS4G

1. Introduction

Climate change has become a severe issue on the planet, with an increase in the average global temperature leading to more frequent and severe weather events [1,2]. This rise in temperature causes ice sheets and glaciers to melt, contributing to sea level rise [3]. With record-breaking temperatures this year in southern states (e.g., Nevada, Arizona, Texas, and Florida [4,5]), coupled with the increasing trend of ocean temperature and unprecedented ice melting speed, an inevitable sea level rise is occurring. A few feet of sea level rise may not sound harmful, but it becomes lethal when combined with king tides and storm surge, especially considering the vast number of people living near the shoreline. According to Small *et al.* [6], approximately 400 million people live within 20 meters of sea level and within 20 km of the coastline worldwide. Sea level rise could result in a series of consequences, such as saltwater intrusion into inland rivers contaminating freshwater resources and harming agricultural lands [7,8]. Coastal ecosystems like mangroves, marshes, and coral reefs can be altered, resulting in the loss of habitats for certain species [9,10]. For human communities, shoreline infrastructure and properties are vulnerable to flooding, and homeowners may be forced to relocate, significantly disrupting the local economy [11]. Thus, to cope with the impact of sea level rise and prepare for future climate change, it is crucial to map the inundation in different sea level rise scenarios.

The remainder of the paper is structured as follows. Section 1.1 gives an overview of related literature, while Section 1.2 explains the novelty of our contribution. Section 2 describes the datasets and algorithms employed in the study. More specifically, Section 2.1 discussess elevation and water surface datasets and related vertical reference systems, while Section 2.2 explains the mapping process. Our FOSS4G (Free and Open-Source Software for Geospatial) implementation is described in Section 2.3, followed by the description of a case study in Section 2.4. Results of a case study demonstrating the approach are presented in Section 3, and finally Section 4 concludes the work and places it into context.

 doi:10.20944/preprints202311.0504.v1

1.1. Previous work

Currently, various models have been used in sea level rise inundation modeling. Based on different spatial scales, complexity of computation, and data involved in the model, SLR models can be generally divided in to Hydrodynamic models and GIS-based approaches [12]. Hydrodynamic models, such as the SLOSH (Sea, Lake, and Overland Surges from Hurricanes) Model tailored to specific shoreline intricacies [13], Delft3D focusing on hydrodynamics and sediment transport [14], and ADCIRC (Advance Circulation Model for Coastal Ocean Hydrodynamics) modeling coastal water levels and currents, aim to replicate the dynamics of water inundation [15]. Although they are effective for predicting hurricane-driven storm surges, these models are constrained to specific areas due to their intricate demands for expertise, data, and computational power. In contrast, GIS-based models are emerging as a more accessible method to map SLR inundation. Requiring decent data quality and computational resources, they are also easily adaptable to various regions [16]. Medium-resolution GIS techniques sufficiently address the needs of scientific research, coastal management, and spatial planning in understanding coastal processes and assessing hazards [12]. Prominent GIS-based models include SLAMM (Sea Level Affecting Marshes Model), which relies on elevation data, BTELSS (Barataria-Terrebonne ecological landscape spatial simulation) addressing regional coastal dynamics [17,18], and the widely-used Bathtub model [19,20]. Williams and Lück-Vogel [12]'s enhanced version of the Bathtub model offers improved accuracy in storm surge contexts by considering additional parameters. Some GIS models, like DIVA, even delve into the broader impacts of SLR, including socioeconomic and biophysical implications, as well as the adaptive strategies' costs and benefits [21,22]. Web applications, such as NOAA's (National Oceonagraphic and Athmospheric Administration) Sea Level Rise Viewer[1] and Climate Central's Coastal Risk Screening Tool[2] are just a few examples that popularize SLR inundation mapping by making SLR scenario maps available to the public.

While multiple examples of flood-related FOSS4G solutions exist ([23–25], most models and studies rely on proprietary software. For example, Lichter and Felsenstein [26] crafted an automated method utilizing ArcGIS geo-processing commands in Python to locally gauge the financial implications of SLR and intense flooding. Li *et al.* [27] and Perini *et al.* [28] both developed their coastal inundation models with the aid of ESRI's Cost-Distance tool, while both models take into account hydrological connectivity to the coastline, and the latter also factors in the beach slope that sea-borne inundation water must traverse. Additionally, NOAA's popular SLR Viewer tool employed ArcGIS software for SLR inundation mapping [29]. While the capabilities of proprietary software undeniably useful for modeling SLR scenarios, their proprietary nature limits broader adoption and utilization.

With the advancement of the open data policy issued by the Office of Management and Budget (OMB) in 2013, accessibility to geospatial data has significantly improved [30]. In the context of U.S. policy, the Federal Geographic Data Committee (FGDC), founded in 1990, aims to promote the coordinated development, utilization, sharing, and dissemination of geospatial data across all governmental levels, the private sector, non-profit entities, and academic institutions [31]. In 2001, the geospatial one-stop initiative introduced a portal for the discovery and retrieval of geospatial assets from various governmental bodies and it has been embraced by professionals, from urban planners and researchers to policymakers, all of whom depend on spatial data for informed decision-making [32]. The Geospatial Data Act of 2018 further emphasized the importance of public accessibility, endorsing data sharing across governmental tiers, all while heeding privacy and security concerns [33]. This act has underscored the principles of collaboration, transparency, and efficiency in geospatial data usage. With the progress made in open data policies, the development of Free and Open Source

[1] https://coast.noaa.gov/digitalcoast/tools/slr.html
[2] https://coastal.climatecentral.org/

 doi:10.20944/preprints202311.0504.v1

Software (FOSS) has also kept pace. The adoption of FOSS offers several advantages, including cost reduction, vendor independence, heightened customizability, assured interoperability, and robust community support. There's been a notable momentum in the geospatial domain towards such open-source paradigms, namely Free and Open Source Software for Geospatial (FOSS4G). FOSS4G's value, particularly in an economic context, has been highlighted in developing nations [34]. Addressing the issue of global coastal inundation, particularly in resource-limited settings, necessitates the creation of an open-source tool for sea level rise inundation mapping. Building on recent open data policies and advancements in free and open software, the groundwork is now laid for crafting a dedicated approach to mapping sea level rise inundation at local scales.

1.2. Contribution and significance of study

This research presents an open-source framework designed to map SLR inundation following NOAA's passive coastal inundation mapping framework [35]. We leveraged various open-source GIS-based tools, including GDAL, QGIS, and GRASS GIS. Beyond the simple bathtub model, our methodology incorporates hydrological connectivity, but due to computing constraints, some influencing factors of SLR are omitted from the model (see limitations in Section 3.4). Harnessing a blend of high-resolution elevation models, tidal data, and projected SLR scenarios, we formulated an integrated workflow using FOSS4G tools to chart inundation extents across diverse SLR situations. Our approach highlight that FOSS4G tools present a viable and economic approach to map SLR inundation. This not only aids stakeholders in gauging coastal vulnerabilities but also helps in shaping resilient adaptation strategies. The adoption of an open-source strategy promotes widespread collaboration and ensures reproducibility, laying the foundation for a more exhaustive understanding of SLR effects on coastal systems.

2. Materials and Methods

To successfully map SLR inundation extents, a variety of data sources are needed throughout the process, which are detailed below.

2.1. Surface and Water Elevation Data

Digital elevation models (DEMs) are the representation of land elevation (topographic) or water depth (bathymetric). These datasets serve as the most valuable resources for coastal mapping applications [36]. The process of SLR inundation mapping deals with the interaction of land and water, and therefore relies on not only topographic and bathymetric elevation, but datasets representing water levels [37]. Since multiple elevation datasets have to be used in the process, the first challenge is maintaining consistency between them in terms of their spatial reference. While horizontal datum transformations are basic functionality in most GIS software, vertical datum transformations are less commonly used. However, to map coastal inundation, all datasets must reference elevations in the same system. These reference systems developed to measure measure heights and depths on Earth's surface are called vertical datums [38]. They can be established using ellipsoidal, orthometric or tidal models. Figure 1a illustrates ellipsoidal model heights (h, N) that use a simplified, geometric surface to represent Earth's shape and size, and orthometric model heights (H), which is a physical, gravimetric model that approximates mean sea level. In the United States, DEMs are created by various government agencies and other actors in varying detail. This includes local, state and federal organizations. An overview of this complex data ecosystem is provided by Juhász *et al.* [39]. While the nationally available 1 arc-second spatial resolution (30 m) National Elevation Dataset is not adequate for accurate coastal inundation mapping, high-resolution datasets are increasingly being created and made available publicly [40]. These provide enough detail that can facilitate coastal and marine spatial planning on localized scales.

Preprints (www.preprints.org) | NOT PEER-REVIEWED | Posted: 8 November 2023 doi:10.20944/preprints202311.0504.v1

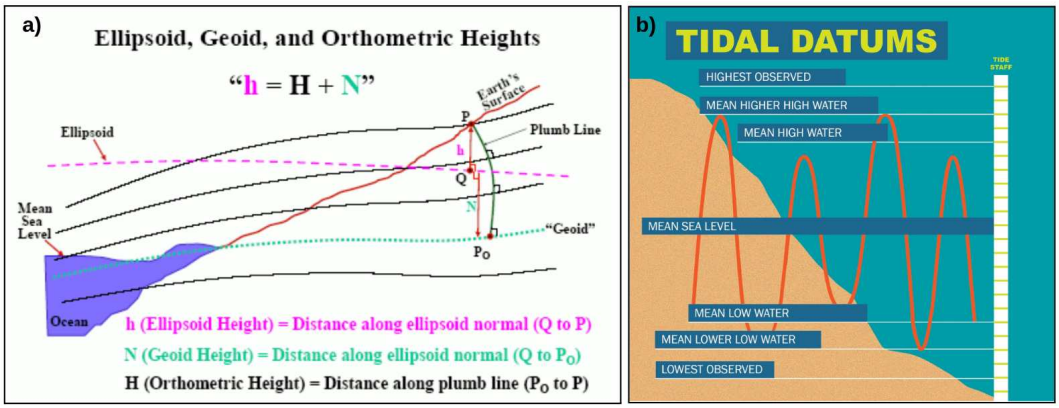

Figure 1. Illustration of referencing elevation data to different vertical datums (a) [35]; and commonly used tidal datums (b) [38]

Tidal datums reference water levels according to certain tidal stages [38]. While geodetic and orthometric datums are more precise and they can be used over a larger area, tidal levels vary by time and by location, therefore tidal datums always refer to one particular location. Figure 1b shows common tidal datums, while Table 1 lists the difference in elevation values of a specific tidal station in Virginia Key, FL. The Mean Higher-High Water (MHHW) is the average height of the highest tide recorded at a station over a period. It is more meaningful for example for land development purposes than lower tidal datums [41], and therefore it is a common reference datum to measure coastal inundation, since areas that are below the MHHW surface are likely to be flooded daily during a normal high tide. For other purposes, such as permitting, other tidal surfaces such as Mean High Water (MHW) are used. Table 1 shows that in Virginia Key, FL, the MHHW surface is 7 cm above the NAVD88 (North American Vertical Datum of 1988) orthometric datum, and 64 cm above the mean sea level at that location. In addition, oceans and seas are not flat surfaces and they deviate locally and regionally due to land movement, varying temperature and other factors [42,43]. This necessitates to integrate accurately representation of tidal surfaces in the inundation mapping process as opposed to using a constant elevation value in modeling inundation extent. A simple, commonly used approach to generate a digital representation of tidal surfaces is using data from tidal stations (see e.g. [44]), however, enough number of tidal gauges must be available to cover the study area. Another approach in the United States is to use VDatum, a database and software developed by NOAA, designed to vertically transform geospatial data among a variety of tidal, orthometric and ellipsoidal vertical datums [45]. However, VDatum covers only the continental United States, Puerto Rico, and the U.S. Virgin Islands, therefore, other areas need to use other approaches to general local tidal surfaces [46]. Software with similar functionality to VDAtum exist for other areas, such as the Australian Coastal Vertical Datum Transformation (AusCoastVDT) Software [47] and Vertical Datum Conversion Tool from the Canadian Geodetic Survey [48].

Preprints (www.preprints.org) | NOT PEER-REVIEWED | Posted: 8 November 2023 doi:10.20944/preprints202311.0504.v1

Table 1. Tidal datums for Virginia Key, Biscayne Bay, FL Tidal Station (#8723214) for Tidal Epoch 1983-2001 along with their relative elevation values compared to Mean Higher-High Water [49]

Datum	Description	Value [m]
Max. Tide	Highest Observed Tide	1.09
MHHW	Mean Higher-High Water	0.00
MHW	Mean High Water	-0.02
NAVD88[1]	North American Vertical Datum of 1988	-0.07
MSL	Mean Sea Level	-0.34
MLW	Mean Low Water	-0.64
MLLW	Mean Lower-Low Water	-0.68
Min. Tide	Minimum Observed Tide	-1.08
STDT	Station Datum	-3.77

[1] NAVD88 is an orthometric datum.

2.2. Bathtub Approach to Mapping SLR Inundation

Coastal areas become flooded as they submerge below surrounding water levels due to the rise in sea levels. This is typically simulated using a "bathtub" approach. This simple model assumes that areas that are below a water reference surface are filled with water like a bathtub. This approach relies on digital representations of the topography (DEM) and water surface, as described is Section 2.1. The process can be formalized as follows:

$$I_{x,y} = \begin{cases} 1 & \text{if } D_{x,y} \leq W_{x,y} \\ 0 & \text{if } D_{x,y} > W_{x,y} \end{cases} \quad (1)$$

where I is a binary variable indicating whether an area is inundated (1) or not inundated (0) at location (x, y), while D and W are the DEM elevation value and projected water level respectively at that location. The bathtub can be "filled" with or without hydrological connectivity. In the latter case, only areas that are connected to the main water body (i.e. ocean or sea) are considered flooded. This can be achieved by multiplying I in Equation 1 by $C_{x,y}$ which represents hydrological connectivity, i.e. whether a location is connected (1) or not connected (0) to the main body of water. Areas where $I_{x,y} \neq (I_{x,y} \times C_{x,y})$ can be considered low-lying.

Modeling SLR inundation in a GIS environment is a multi-step process that is usually computed using a combination of standard, cell-based raster operations. While most commonly used desktop GIS software do not have a dedicated tool to perform this task, the process is well-documented and has been described before (see e.g. [50]). A general flowchart is given in Figure 2. The process relies on three inputs, a raster DEM representing elevation values, a baseline raster surface representing the surface on which SLR is measured, and and a numerical SLR value that represents the rise in sea levels above that reference surface. MHHW is commonly used as a baseline surface (tidal surface), since it is a reliable reference point for understanding the upper limits of daily tidal fluctuations. We refer to SLR scenario as an x *meter* increase in sea levels above MHHW. The process starts by creating an increased water surface that is x m above the baseline surface (step 1). With reference to Equation 1, $W = t + x$, where t is the tidal surface. This new surface W represents the water surface in the bathtub modeling process to which the topography (DEM) is compared to. Next, the water surface is subtracted from the DEM (step 2). This resulting surface is negative if the water surface is below the DEM. In step 3, a cell-based classification is performed that classifies this surface into a binary map where cell values of 1 represent areas that fall below the water surface, in other words, "bathtubs" filled with water. Hydrological connectivity is evaluated in steps 4-6, where the binary map produced in step 3 is first recategorized by grouping cells that form physically discrete areas together. Then, categories that represent inundated areas connected with the main body of water are retained. This surface is identical to I in Equation 1. Subsequent steps are optional, but can be used for specific purposes. For example projected water depths can be generated by using I as a mask surface to overlay with the

Preprints (www.preprints.org) | NOT PEER-REVIEWED | Posted: 8 November 2023 doi:10.20944/preprints202311.0504.v1

water depth surface generated in step 2. Additionally, a raster to vector conversion can be used to extract inundation polygons to use in vector-based spatial operations and visualization (step 8).

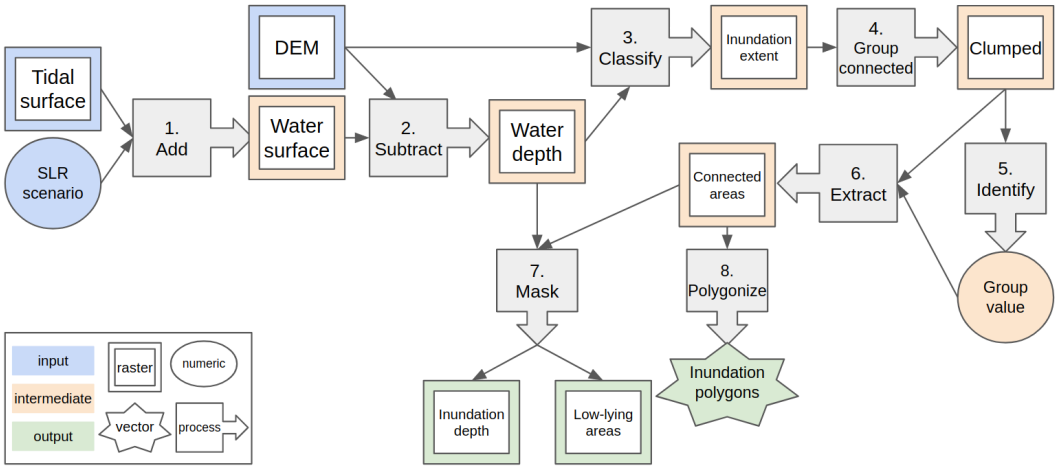

Figure 2. General workflow of the SLR mapping process

2.3. FOSS4G Implementation

While the implementation of the bathtub approach has been described before, it has been mainly done with proprietary tools, such as the ESRI ArcGIS suite of software [29,46,50]. In this section, we describe an alternative environment that utilizes FOSS4G software tools to implement bathtub modeling of SLR inundation.

2.3.1. Software and Tools

Our implementation uses three widely used FOSS4G software, namely the Geospatial Data Abstraction Library with the OGR Simple Features Library (GDAL/OGR), Geographic Resources Analysis Support System (GRASS GIS) and QGIS. These software frameworks represent an ensemble of geospatial tools and algorithms, each purpose-built to excel in specific geospatial tasks such as raster algebra, vectorization, data transformation, and more. It is the seamless integration and collaboration among these tools and algorithms that culminate in the creation of a comprehensive desktop GIS software solution.

In essence, GDAL/OGR[3] provides abstract data models to represent raster and vector geospatial data. It also contains useful utility tools to translate between formats as well as to process data [51]. GDAL/OGR facilitates seamless integration into scientific workflows, enabling spatial data professionals to efficiently manage and extract meaningful insights from complex geospatial datasets.

GRASS GIS[4] is a multi-purpose GIS software used for the production, analysis and presentation of geospatial data. It is one of the most comprehensive GIS software available, with its development work dating back to 1982 [52]. With an extensive array of tools for raster and vector data processing, terrain analysis, hydrological modeling, and more, GRASS GIS provides the means to conduct geospatial analyses, all within a flexible and customizable environment. Its integration of geostatistical, image analysis, and visualization capabilities renders it as an indispensable tool for spatial research.

QGIS[5] is a desktop GIS software widely employed in scientific research due to its robust geospatial data handling capabilities and extensive analytical tools [53]. Offering a user-friendly interface, QGIS enables researchers to visualize, analyze, and manipulate spatial data. Its adaptability through plugins

[3] https://gdal.org
[4] https://grass.osgeo.org
[5] https://qgis.org

Preprints (www.preprints.org) | NOT PEER-REVIEWED | Posted: 8 November 2023 doi:10.20944/preprints202311.0504.v1

and support for numerous data formats further enhances its utility, facilitating complex geospatial analyses and fostering collaborative scientific exploration. In addition to its native algorithms, QGIS also provides an interface to run GDAL/OGR and GRASS GIS algorithms.

All three software are relased as open-source software and are official projects of the Open Source Geospatial Foundation (OSGeo[6]), which is an umbrella organization that fosters the development and promotion of open-source geospatial technologies and supports collaborative efforts within the geospatial community.

Table 2 relates the general workflow described in Figure 2 to specific software and algorithms. Specific implementation of these steps in the context of the case study presented in Sections 2.4 and 3 are given in Appendix A and are also provided[7].

Table 2. Steps of SLR inundation mapping workflow with FOSS4G tools

Step	Description	Input(s)	Output(s)	Software	Tool
1	Add SLR scenario to tidal surface raster	Tidal surface (raster) SLR value (numeric)	Water surface (raster)	GDAL	gdal_calc
2	Subtract DEM from water surface	Water surface (raster) DEM	Inundation depth (raster)	GDAL	gdal_calc
3	Create inundation extent	Inundation depth (raster) DEM	Binary water extent (raster)	GDAL	gdal_calc
4	Group connected cells	Binary water extent (raster)	Clumped (raster)	GRASS GIS	r.clump
5	Identify hydrologically connected areas	Clumped (raster)	Max value (numeric)	QGIS GDAL	identify gdalinfo
6	Extract hydrologically connected water surface	Clumped (raster) Max value (numeric)	Connected areas (raster)	GDAL	gdal_calc
7	Conflate water depth with inundation mask	Connected areas (raster) Water depth (raster)	Inundation depth (raster) Low-lying areas (raster)	GDAL	gdal_calc
8*	Polygonize inundation extent	Inundated areas (raster)	Inundation areas (vector)	GRASS GIS GDAL/OGR	r.to.vect ogr2ogr

* Optional steps.

2.3.2. Software Interfaces

These software and tools presented in the previous section can be interfaced in various ways. GDAL/OGR, QGIS and GRASS GIS all provide application programming interfaces (APIs) that allows to integrate their algorithms in custom-built software. However this can be considered advanced use-case, and for end uses, such as GIS analysts and coastal professionals, this is usually not necessary. More convenient ways to access functionality necessary for coastal inundation mapping are through graphical user interfaces (GUIs), such as desktop software environments, and through the command line.

2.4. Description of the Case Study

We demonstrate the implementation with a case study in Virginia Key, which is an approximately 3.5km^2 barrier island in Miami, FL, USA. The island constitutes of a mix of built-up and natural areas, and houses the Miami Seaquarium and a wastewater facility, as well as is home to large mangrove wetlands. A NOAA tidal station (#8723214[8]) is located on southern part of the island. We adapt the extrapolated intermediate sea level scenario specific to this location for the year 2060. The amount of SLR is 0.44 m (1.44 ft). In the USA, this can be determined for each tidal station with sufficient observations using the Interagency Sea Level Rise Scenario Tool maintained by NASA[9]. Other scenarios

6 https://osgeo.org
7 https://doi.org/10.17605/OSF.IO/XEPGR
8 https://tidesandcurrents.noaa.gov/stationhome.html?id=8723214
9 https://sealevel.nasa.gov/task-force-scenario-tool?psmsl_id=1858

Preprints (www.preprints.org) | NOT PEER-REVIEWED | Posted: 8 November 2023 doi:10.20944/preprints202311.0504.v1

and detailed methodological description of determining SLR are given by Sweet *et al.* [54]. The other main input is a LiDAR-based, bare-earth, hydro-enforced DEM provided by Miami-Dade County from 2021 [55]. Elevation values are referenced in meters in relation to NAVD88.

Since areas below the MHHW are susceptible to inundation, we use this surface to identify inundated areas. MHHW is determined at the Vriginia Key tidal station, and is 0.07m above the NAVD88 reference surface [49]. However, the ocean is not a flat surface, and there can be significant amount of variation in the height of tidal surfaces [56]. For this reason, we sampled MHHW at multiple locations and interpolate a continuous tidal surface using these distinct points. MHHW was also expressed in meters in reference to NAVD88. Chapter 3 demonstrates this process for Virginia Key. Step-by-step instructions are provided in Appendix A.

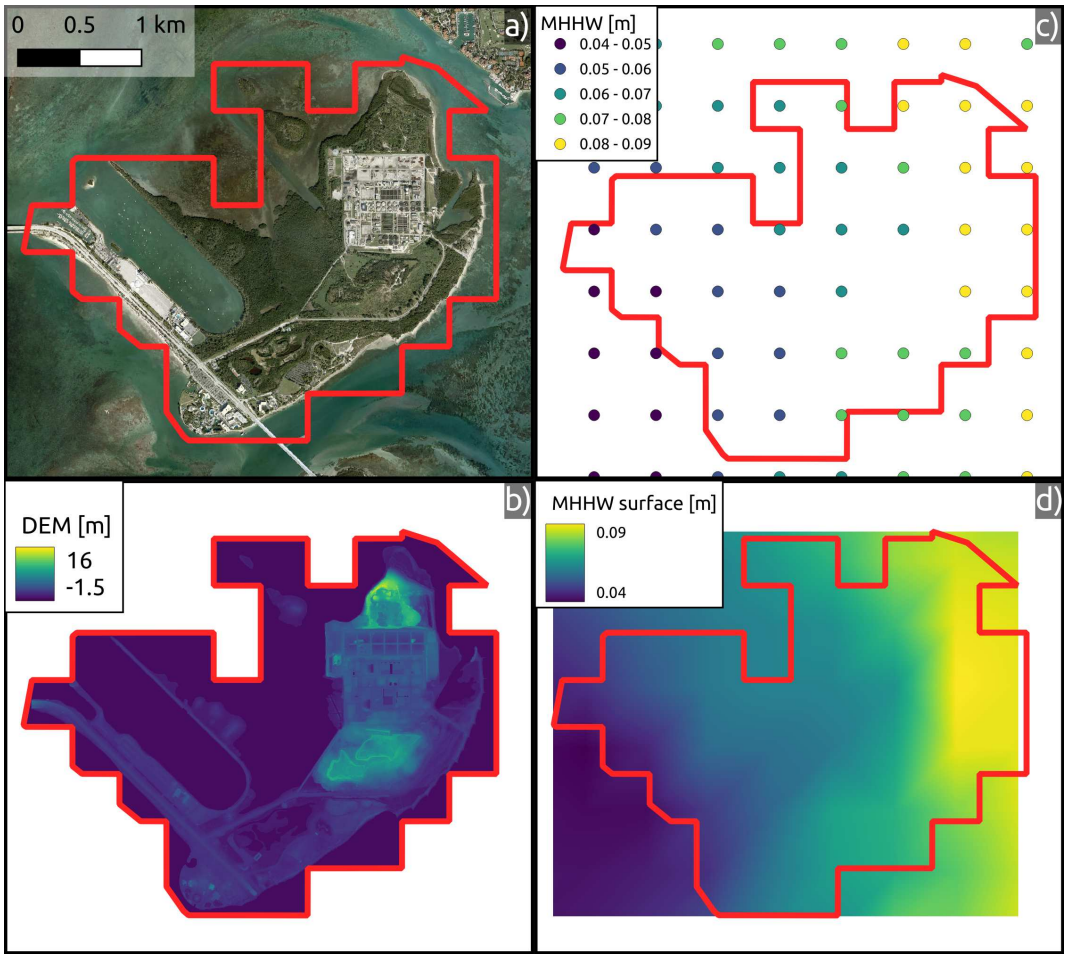

Figure 3. Satellite photo of the Virginia Key study area (red outline) (a); LiDAR-based DEM of the study area with NAVD88 elevations (b); Locations where MHHW was sampled (NAVD88) (c); and interpolated, continuous MHHW surface (d)

3. Results

The following section describes our FOSS4G approach for the Virginia Key Study areas. Throughout the section, references to specific steps in Figure 2 are also given.

3.1. Preparation of the Datasets

As described in Section 2.1, coastal inundation modeling requires high quality input elevation datasets that represent various surfaces. The DEM representing ground elevations was reprojected to the North American Datum 1983 (NAD83) / Universal Transverse Mercator (UTM) zone 17N coordinate system and resampled to 2.5 m pixel resolution. This resolution balances computational

Preprints (www.preprints.org) | NOT PEER-REVIEWED | Posted: 8 November 2023 doi:10.20944/preprints202311.0504.v1

efficiency and results, and is considered adequate for local-scale modeling of inundation. The study area and the corresponding DEM is shown in Figure 1a-b. The difference in elevation within the study area is 17m between the lowest and highest points. The highest elevation area are located within the coastal dunes of the northern tip of the island.

While a common approach is using the MHHW surface value from the nearest tidal station as reference, we recognize that MHHW varies in space. We use NOAA's VDatum software to sample MHHW at distinct locations shown in Figure 1c around the study area. VDatum is able to convert between various orthometric and tidal datums. We express MHHW in reference to NAVD88 so that the elevations can be directly compared with the DEM. Figure A3 shows the correct setup to transform MHHW to NAVD88 values in VDatum. It has to be noted that VDatum coverage area does not extend far beyond the shoreline. Unlike our study area, coastal mapping projects may aim to extend inland, which requires special steps to extend the tidal surface inland as well [29,57]. In the next step, we use the TIN (triangulated irregular network) approach to interpolate a continuous surface using the same spatial reference and pixel size as the DEM. TIN is an exact interpolation technique that retains the sampled values at those locations, and returns the interpolated elevation value based on linear interpolation between the sampled points within each triangle of the network. The interpolated surface is shown in Figure 1d. The difference between MHHW is 5cm between the Biscayne Bay and Atlantic sides of the study area. While this seems negligible, it already represents 11% of the projected SLR value in 2060. In addition, the difference over larger study areas can be more significant, which highlights the importance of using a more refined MHHW surface than using a constant value across the entire study area.

After preparing these datasets, all inputs of the modeling approach (see Figure 2 are available. The SLR value for the intermediate scenario in 2060 is 0.44m. The DEM and the MHHW surface are available as single-band rasters in the NAD83 / UTM Zone 17N coordinate system with 2.5 m pixel resolution, pixel values representing MHHW elevations above NAVD88 orthometric datum.

3.2. Simulating SLR Inundation

The SLR scenario value (0.44 m) can be added to the interpolated MHHW surface using cell-based raster algebra. The new water surface represents MHHW in 2060 according to the intermediate SLR scenario (step 1). Equation 1 is implemented in two steps, first by subtracting the new water surface (W) from the DEM (D) (step 2), then evaluating pixel values to determine inundation extent (step 3). Figure 4a shows inundation depth after step 2. Since areas where $D > W$ cannot be considered inundated, these values are retained as 0. In step 3, a binary map is created where negative values are reclassified and given the value of 1, representing areas that are below the SLR scenario (Figure 4b). The previous steps are executed using raster algebra which is usually implemented in both FOSS and GIS software. GDAL provides a command-line interface through the *gdal_calc* python script[10]. This is also accessible from the QGIS GUI in addition to QGIS' own implementation.

Next, hydrological connectivity is evaluated. Pixels in the the binary water extent map generated in step 3 (Figure 4b) take the value of 1 if the pixel is below the SLR scenario (hence potentially inundated) or 0 if it lies above the SLR scenario (i.e. not inundated). Neighboring inundated cells can be grouped together to form physically distinct areas with the *r.clump* GRASS GIS algorithm (step 4). This tool finds all contiguous areas of the same cell value and assigns a unique category to these areas (also referred to as "clumps"). Figure 4c illustrates clumps within the study area. Unique categories are distinguished with different colors. In this figure, the category representing the main body of water is shown in purple with the category ID 538. Identifying this category is a manually process and can be done in the QGUS GUI through the *Identify* tool (step 5).

---

[10] https://gdal.org/programs/gdal_calc.html

Preprints (www.preprints.org) | NOT PEER-REVIEWED | Posted: 8 November 2023 doi:10.20944/preprints202311.0504.v1

Once the category number of the water body is identified in the clumped map, this area can be used to extract hydrologically connected areas (step 6). This is done by reclassifying the clumped raster map into a binary map using *gdal_calc*. The result map is shown in Figure 4d. The difference between this output and the previously created map in Figure 4b is that inland areas below the SLR scenario are removed.

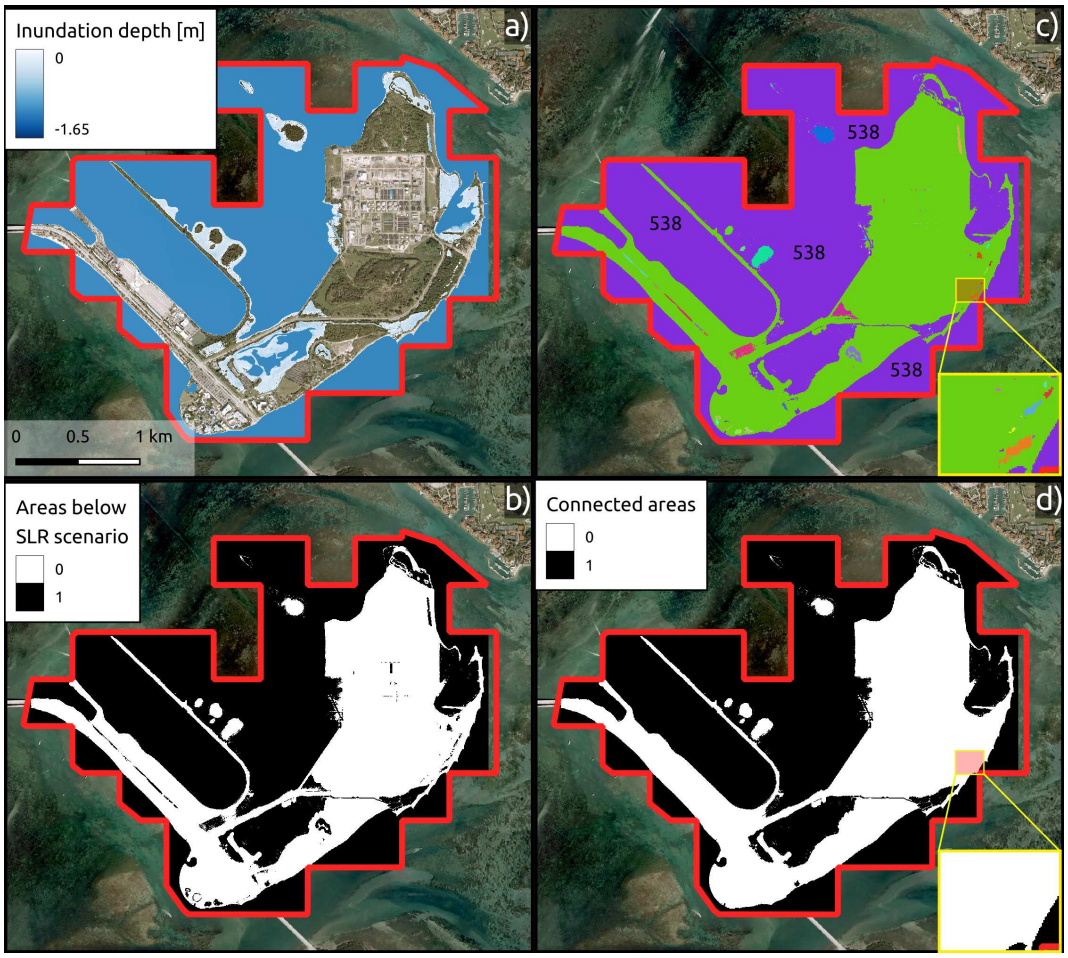

Figure 4. Inundation depth is calculated by subtracting a SLR scenario from the DEM of the study area (a); Binary map showing pixels below SLR-increased MHHW (b); grouping cells that form physically discrete areas into 'clumps' (c); binary inundation map representing areas that are hydrologically connected to the main body of water (d)

In step 7, the connected areas raster layer can be used as a mask to extract low-lying areas, that are below the SLR scenario but not hydrologically connected, as well as to exclude these areas from the inundation depth raster created earlier in step 2 (Figure 4a).

In step 8, raster-vector conversion is performed on the binary inundation map from step 3 and the connected areas map from step 6. This conversion is done using the *r.to.vect* function available in GRASS GIS. The conversion process transforms the low-lying areas and the hydrologically connected areas from binary rasters into vector polygons. These vector datasets are more suitable for certain spatial analyses and can be integrated with other vector-based datasets for a comprehensive assessment. Other advantages of the vector format in this context is the potentially smaller size of the dataset over larger areas as well as vector-based visualization techniques. Visualization options are explored in Section 3.3 below. its

Preprints (www.preprints.org) | NOT PEER-REVIEWED | Posted: 8 November 2023 doi:10.20944/preprints202311.0504.v1

3.3. Visualization of SLR and Low-Lying Areas

Figure 5a-b show the study area with and without displaying coastal inundation under the 2060 intermediate SLR scenario (+0.44 m). SLR inundation is usually visualized using pre-rendered outputs similar to Figure 4a and Figure 4e. There are two main approaches. First, similarly to Figures 4a and 5c, inundation depth can be displayed with graduated colors. This approach is popularized by NOAA's Sea Level Rise Viewer[11] [58] that can display SLR for the contiguous United States. Furthermore, NOAA also allows to integrate these visuals in other application through serving the data through application programming interfaces (APIs), OGC (Open Geospatial Consortium) compliant services and ESRI-compatible maps. This allows other users to ingest SLR visualizations within their own GIS system [58]. A similar approach shown in Figure 5d displays pre-rendered, cell-based raster images using a single color to represent inundated areas. Low-lying areas can be displayed with both of these approaches.

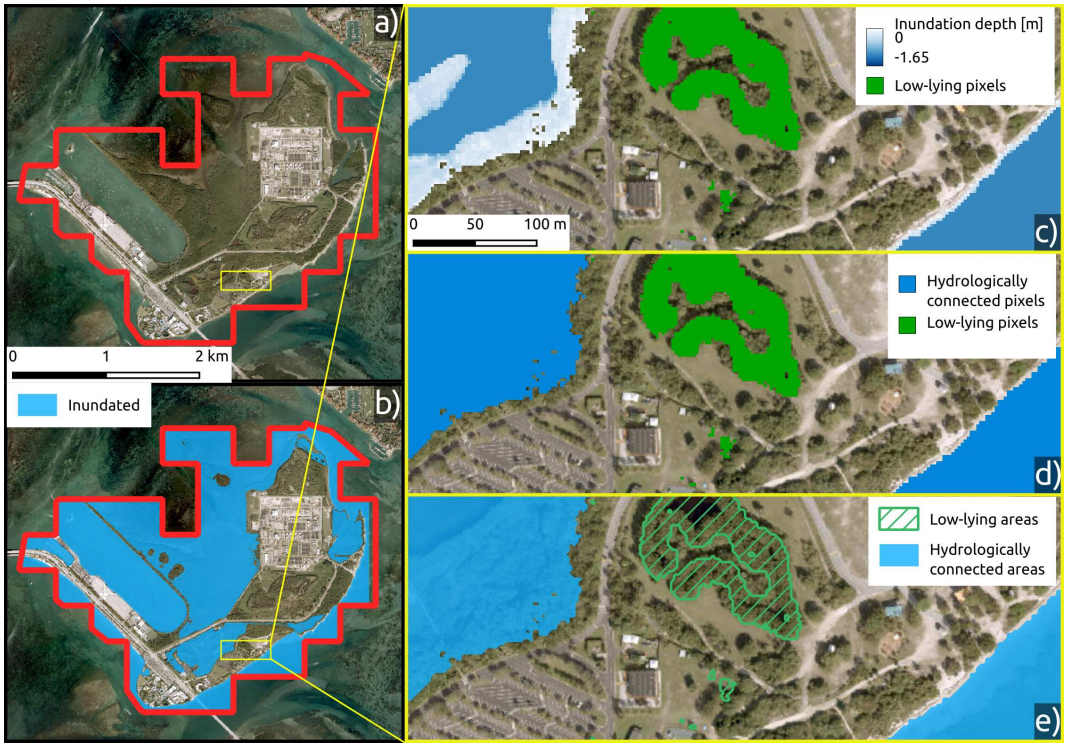

Figure 5. Satellite view of Virginia Key, FL (a); Inundated areas in Virginia Key under the 2060 intermediate scenario (+0.44 m) (b); and SLR visualization methods using: graduated colors (raster) (c); simple colors (raster) (d) and vector polygons (e)

As described in Section 3.2, inundated and low-lying areas can also be converted into vector polygons, which opens up the flexibility of visualizing vector datasets. An example is given in Figure 5e, where in addition to the semi-transparent inundation polygon, low-lying areas are symbolized with dashed polygons. Outside of desktop GIS environments, the flexibility of vector visualization can be exploited in interactive web applications that show the impact of SLR [39].

3.4. Limitations of the Bathtub Mapping Approach

While the passive inundation modeling approach provides a valuable tool for understanding potential flood risks in various scenarios, it has its inherent limitations. These are given below:

[11] https://coast.noaa.gov/slr/

 doi:10.20944/preprints202311.0504.v1

- The approach relies on static input data, however, over time, natural and artificial processes can significantly alter the landscape, potentially leading to inaccurate flood predictions.
- The approach doesn't consider the dynamic interplay of water flow, wave action, and wind. This can lead to an oversimplification of flood scenarios, especially in areas prone to storm surges or rapidly changing water levels.
- We assume universal rise in water levels across the entire study domain, however factors such as tidal variations, river discharges, and localized rainfall can cause significant disparities in water level changes across a region. This is more prominent over large study areas
- The accuracy and resolution of the data inputs, such as DEMs directly impact the reliability of passive inundation models

It is essential for researchers and policymakers to recognize these limitations when interpreting results from passive inundation models. While they offer valuable insights, they should ideally be used in conjunction with other modeling techniques and real-world data for a comprehensive understanding of flood risks.

4. Discussion and Conclusions

The escalating threat of sea level rise due to climate change underscores the need for accurate and accessible tools to predict and visualize potential inundation scenarios. Historically, most studies and applications in this domain have relied heavily on proprietary tools, which often come with significant costs and limited accessibility. This creates barriers, especially for stakeholders in developing nations where resources are constrained, and the need for such tools is pressing.

Our study bridges this gap by presenting a comprehensive methodology for mapping SLR inundation using the bathtub approach, but with a distinct emphasis on leveraging the capabilities of free and open-source tools. This democratizes the inundation mapping process, making it accessible to a broader range of users, from researchers in resource-limited settings to local governments in developing nations. The case study of Virginia Key not only demonstrated the practical application of this approach but also emphasized the importance of accounting for spatial variations in tidal surfaces.

While the results derived from the bathtub model provide valuable insights, they are inherently constrained by the static nature of the input data and the absence of dynamic hydrological considerations. However, the adaptability and cost-effectiveness of FOSS4G tools ensure that the generated outputs can be tailored to diverse audiences, from policymakers to local communities.

In conclusion, our work offers a significant contribution by providing an alternative to proprietary tools for SLR inundation mapping. By harnessing the power of FOSS4G tools, we present a solution that is both accessible and customizable, catering especially to those in resource-limited settings. As the global community confronts the challenges of climate change, such tools will be pivotal in driving informed decision-making and fostering proactive adaptation strategies.

Author Contributions: Conceptualization, L.J. and R.W.P.; methodology, L.J.; software, L.J.; validation, L.J.; formal analysis, L.J.; investigation, L.J. and J.X.; resources, L.J. and R.W.P.; data curation, L.J.; writing—original draft preparation, L.J. and J.X.; writing—review and editing, L.J., J.X. and R.W.P.; visualization, L.J. All authors have read and agreed to the published version of the manuscript.

Funding: This research was supported by the United States Environmental Protection Agency Wetland Development Grant Program (#02D16822).

Data Availability Statement: Sample data and software are available from here: https://doi.org/10.17605/OSF.IO/XEPGR.

Conflicts of Interest: The authors declare no conflict of interest.

Appendix A. FOSS4G implementation

The dataset as well as two Bash scripts that combine the steps described below are available (https://doi.org/10.17605/OSF.IO/XEPGR). The examples are designed to run on Ubuntu 22.04 operating system. All software used in the study are platform-independent, and can run on any

Preprints (www.preprints.org) | NOT PEER-REVIEWED | Posted: 8 November 2023 doi:10.20944/preprints202311.0504.v1

operating system including Microsoft Windows and macOS. Specific software versions are given below.

- **QGIS** 3.34.0-Prizren
- **GRASS GIS** 7.8.7
- **GDAL/OGR** 3.4.1

Our implementation in the case study utilized the command-line interfaces of these software, except for step 5, which was done manually in the QGIS GUI. However, all steps can be run purely in a desktop environment as well. This is illustrated below for Step 1, and can be replicated by the user for the consecutive steps if desired.

Appendix A.1. Step 1

```
gdal_calc.py --co COMPRESS=DEFLATE --calc=A+0.44 \
    --outfile=water_surface.tif -A tidal_surface_navd88.tif
```

The command above adds 0.44 (amount of SLR scenario in meters) to the input raster *tidal_surface_navd88.tif* using cell-based raster algebra. The `-A` flag specifies the input dataset, the `--calc` parameter contains the raster algebra expression, in this case a simple addition operation. The `-co COMPRESS=DEFLATE` flag applies the DEFLATE losless compression method to the output GeoTIFF. Figure A1 illustrates how to run the same tool within the QGIS GUI.

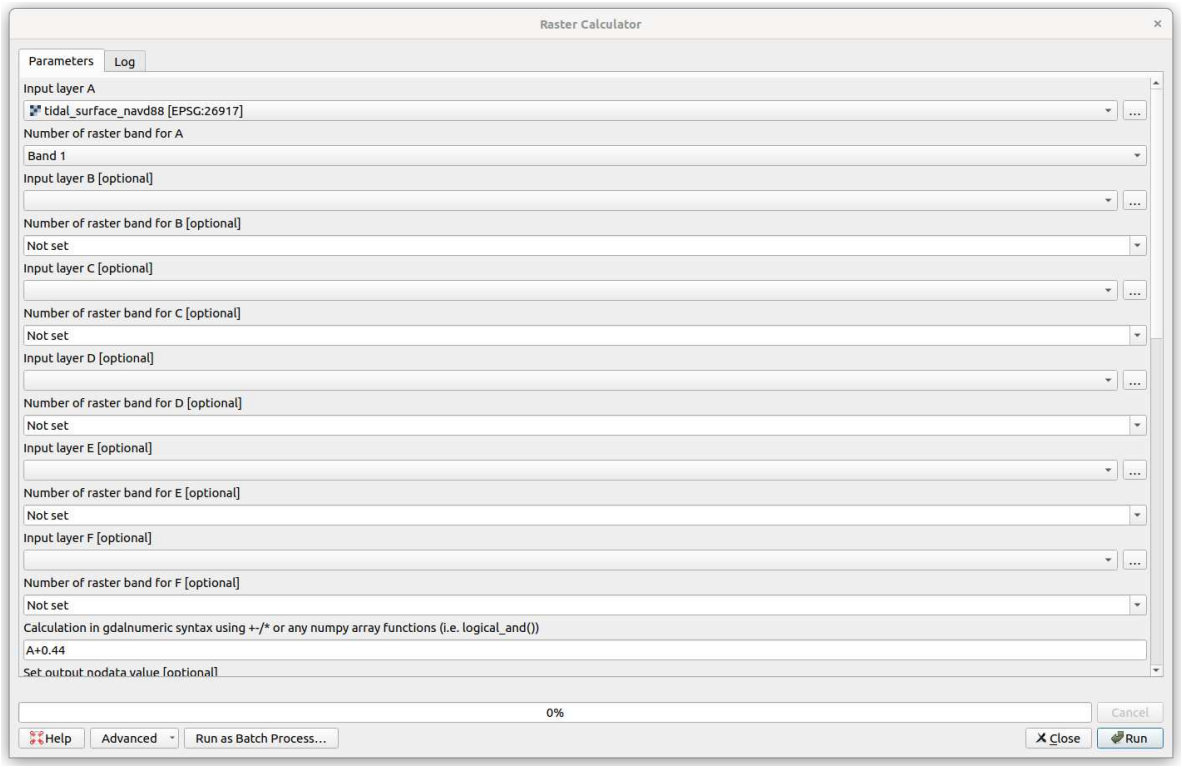

Figure A1. Running *gdal_calc* in QGIS

Appendix A.2. Step 2

```
gdal_calc.py --co COMPRESS=DEFLATE --calc="(A <= B) * (A - B)" \
    --outfile=depth.tif -A project_dem_metric.tif \
    -B water_surface.tif
```

Preprints (www.preprints.org) | NOT PEER-REVIEWED | Posted: 8 November 2023 doi:10.20944/preprints202311.0504.v1

The command above uses the DEM (*project_dem_metric.tif*) and the output of step 1 (*water_surface.tif*) labeled as `A` and `B` respectively. The expression evaluates whether the DEM <= MHHW increase with the SLR scenario, and if so, subtracts these values resulting in the water depth. All other values are retained as 0s since the logical multiplier `A <= B` evaluates to 0.

Appendix A.3. Step 3

```
gdal_calc.py --co COMPRESS=DEFLATE --calc="(A <= B) * 1" \
    --outfile=single.tif -A project_dem_metric.tif \
    -B water_surface.tif
```

Instead of retaining water depth, this command generates a binary water extent raster.

Appendix A.4. Step 4

```
qgis_process run grass7:r.clump --distance_units=meters \
    --area_units=m2 --ellipsoid=EPSG:7019 --input=single.tif \
    --title=clumped.tif ---d=true --output=clumped.tif \
    --threshold=0 --GRASS_REGION_CELLSIZE_PARAMETER=0 \
    --GRASS_RASTER_FORMAT_OPT='COMPRESS=DEFLATE'
```

Grouping connected cells is done by running the *r.clump* GRASS GIS algorithm. Although GRASS GIS can be run natively, this command above uses the QGIS Process Executor engine. The advantage of this approach is that data conversion from GeoTIFF to GRASS' native format and other settings are handled automatically.

Appendix A.5. Step 5

The water surface can be visually identified in QGIS using the *Identify* tool (Figure A2. In the case study, this corresponds to the value of 538.

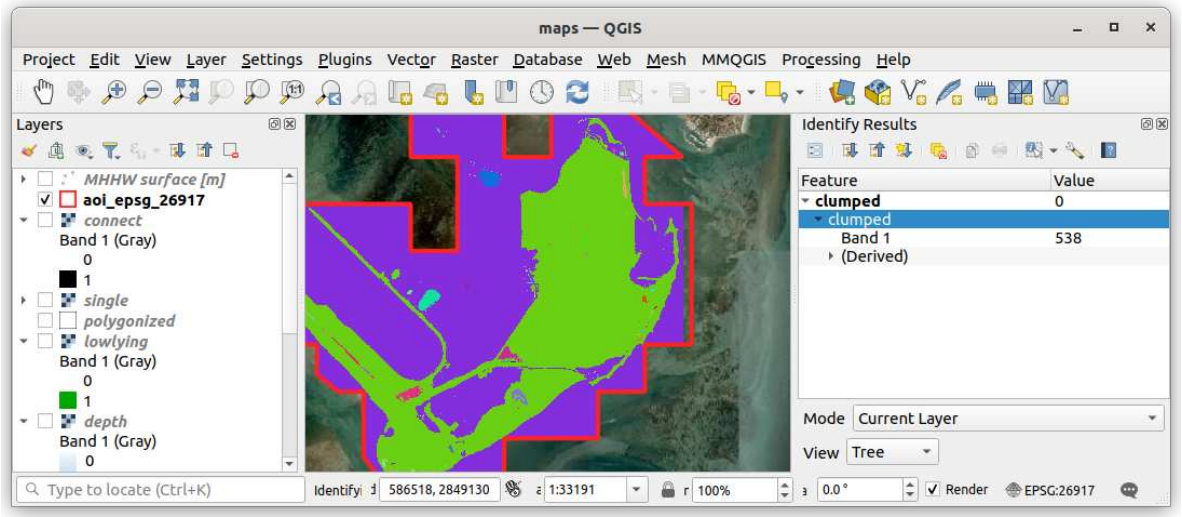

Figure A2. Identifying the category representing the water extent in QGIS.

Appendix A.6. Step 6

```
gdal_calc.py --NoDataValue "65535" --co COMPRESS=DEFLATE \
    --calc="(A == 538) * 1" --outfile=connect.tif -A clumped.tif
```

The command above uses the category identified in the previous step. It retains pixels with the value of 1 if they belong to the hydrologically connected main body of water. All other pixels are classified as 0.

Preprints (www.preprints.org) | NOT PEER-REVIEWED | Posted: 8 November 2023 doi:10.20944/preprints202311.0504.v1

Appendix A.7. Step 7

```
gdal_calc.py --NoDataValue "65535" --co COMPRESS=DEFLATE \
    --calc="(A == 1) * (B == 0) " --outfile=lowlying.tif \
    -A single.tif -B connect.tif
```

The command above retains low-lying areas with the pixel value of 1 by comparing the hydrologically connected output from the previous step with areas that are below the SLR scenario (step 3).

Appendix A.8. Step 8

```
qgis_process run grass7:r.to.vect --distance_units=meters \
    --area_units=m2 --ellipsoid=EPSG:7019 --input=connect.tif \
    --type=2 --column=value ---s=true ---v=false ---z=false \
    ---b=false ---t=false --output=polygonized.shp \
    --GRASS_REGION_CELLSIZE_PARAMETER=0 \
    --GRASS_OUTPUT_TYPE_PARAMETER=3 --GRASS_VECTOR_DSCO= \
    --GRASS_VECTOR_LCO= --GRASS_VECTOR_EXPORT_NOCAT=false

ogr2ogr -where "\"cat\" = 1" inundated.shp polygonized.shp
```

In a 2-step process, first the GRASS GIS algorithm *r.to.vect* is used to convert the hydrologically connected raster dataset into an ESRI shapefile. Then, *ogr2ogr* can be used to retain only the polygons that were created with inundated pixels.

Preprints (www.preprints.org) | NOT PEER-REVIEWED | Posted: 8 November 2023 doi:10.20944/preprints202311.0504.v1

Appendix B. VDatum

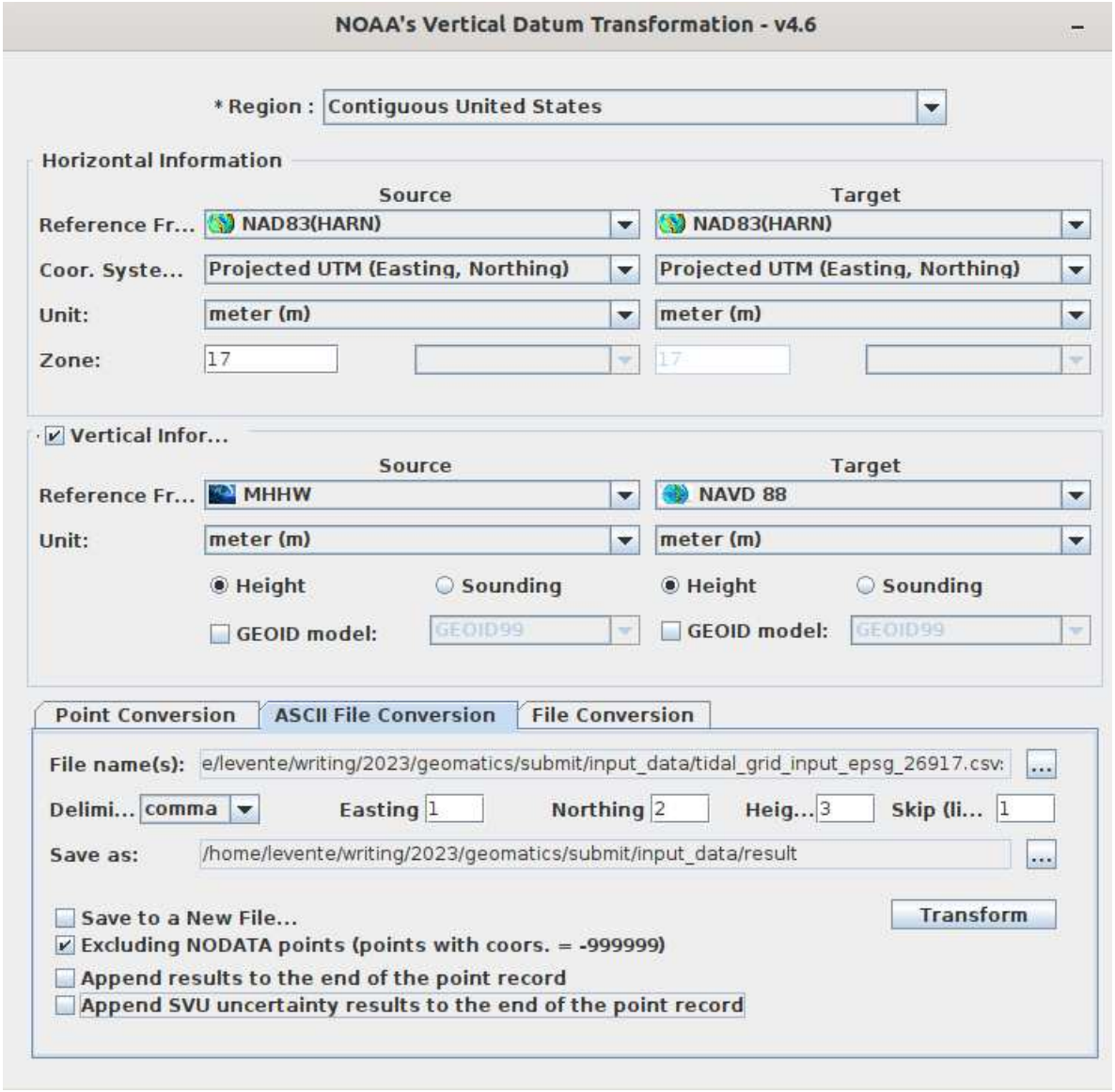

Figure A3. Converting local MHHW grid to NAVD88 elevations using VDatum

References

1. Sobel, A.H.; Camargo, S.J.; Hall, T.M.; Lee, C.Y.; Tippett, M.K.; Wing, A.A. Human influence on tropical cyclone intensity. *Science* **2016**, *353*, 242–246. Publisher: American Association for the Advancement of Science, doi:10.1126/science.aaf6574.
2. Xi, D.; Lin, N.; Gori, A. Increasing sequential tropical cyclone hazards along the US East and Gulf coasts. *Nature Climate Change* **2023**, *13*, 258–265. Number: 3 Publisher: Nature Publishing Group, doi:10.1038/s41558-023-01595-7.
3. Overland, J.; Dunlea, E.; Box, J.E.; Corell, R.; Forsius, M.; Kattsov, V.; Olsen, M.S.; Pawlak, J.; Reiersen, L.O.; Wang, M. The urgency of Arctic change. *Polar Science* **2019**, *21*, 6–13. doi:10.1016/j.polar.2018.11.008.
4. Bushard, B. Record-Breaking Summer: Jacksonville, Miami Break Daily High Temperature Records, After Hottest July Ever. https://www.forbes.com/sites/brianbushard/2023/08/09/miami-phoenix-new-orleans-break-daily-high-temperature-records-heres-where-else-daily-records-have-fallen. Forbes.
5. Fortin, J.F.; Gahan, M.B. Phoenix Breaks Heat Record Set in 1974. https://www.nytimes.com/2023/07/18/us/phoenix-heat-record.html. The New York Times.

6. Small, C.; Gornitz, V.; Cohen, J.E. Coastal hazards and the global distribution of human population. *Environmental Geosciences* **2000**, *7*, 3–12. doi:10.1046/j.1526-0984.2000.71005.x.
7. Ketabchi, H.; Mahmoodzadeh, D.; Ataie-Ashtiani, B.; Simmons, C.T. Sea-level rise impacts on seawater intrusion in coastal aquifers: Review and integration. *Journal of Hydrology* **2016**, *535*, 235–255. doi:10.1016/j.jhydrol.2016.01.083.
8. Snoussi, M.; Ouchani, T.; Niazi, S. Vulnerability assessment of the impact of sea-level rise and flooding on the Moroccan coast: The case of the Mediterranean eastern zone. *Estuarine, Coastal and Shelf Science* **2008**, *77*, 206–213. doi::10.1016/j.ecss.2007.09.024.
9. Daniels, R.C.; White, T.W.; Chapman, K.K. Sea-level rise: destruction of threatened and endangered species habitat in South Carolina. *Environmental Management* **1993**, *17*, 373–385.
10. Parkinson, R.W.; Wdowinski, S. Accelerating sea-level rise and the fate of mangrove plant communities in South Florida, U.S.A. *Geomorphology* **2022**, *412*, 108329. doi:10.1016/j.geomorph.2022.108329.
11. French, G.T.; Awosika, L.F.; Ibe, C. Sea-level rise and Nigeria: potential impacts and consequences. *Journal of Coastal Research* **1995**, pp. 224–242.
12. Williams, L.L.; Lück-Vogel, M. Comparative assessment of the GIS based bathtub model and an enhanced bathtub model for coastal inundation. *Journal of Coastal Conservation* **2020**, *24*, 23. doi:10.1007/s11852-020-00735-x.
13. Jelesnianski, C.P. *SLOSH: Sea, lake, and overland surges from hurricanes*; Vol. 48, US Department of Commerce, National Oceanic and Atmospheric Administration . . . , 1992.
14. Roelvink, J.; Van Banning, G. Design and development of DELFT3D and application to coastal morphodynamics. *Oceanographic Literature Review* **1995**, *11*, 925.
15. Luettich, R.A.; Westerink, J.J.; Scheffner, N.W.; others. ADCIRC: an advanced three-dimensional circulation model for shelves, coasts, and estuaries. Report 1, Theory and methodology of ADCIRC-2DD1 and ADCIRC-3DL **1992**.
16. Mcleod, E.; Poulter, B.; Hinkel, J.; Reyes, E.; Salm, R. Sea-level rise impact models and environmental conservation: A review of models and their applications. *Ocean & Coastal Management* **2010**, *53*, 507–517. doi:10.1016/j.ocecoaman.2010.06.009.
17. Reyes, E.; White, M.L.; Martin, J.F.; Kemp, G.P.; Day, J.W.; Aravamuthan, V. Landscape modeling of coastal habitat change in the Mississippi Delta. *Ecology* **2000**, *81*, 2331–2349. doi:10.2307/177118.
18. Martin, J.F.; White, M.L.; Reyes, E.; Kemp, G.P.; Mashriqui, H.; Day Jr, J.W. Evaluation of Coastal Management Plans with a Spatial Model: Mississippi Delta, Louisiana, USA. *Environmental Management* **2000**, *26*. doi:10.1007/s002670010075.
19. Feenstra, J.F. Handbook on methods for climate change impact assessment and adaptation strategies **1998**.
20. Cartwright, A.; Brundrit, G.; Fairhurst, L. Global climate change and adaptation–A sea-level rise risk assessment. *Phase four: Adaptation and risk mitigation measures for the City of Cape Town. Prepared for the City of Cape Town by LaquaR Consultants CC* **2008**.
21. Hinkel, J.; Nicholls, R.J.; Vafeidis, A.T.; Tol, R.S.; Avagianou, T. Assessing risk of and adaptation to sea-level rise in the European Union: an application of DIVA. *Mitigation and Adaptation Strategies for Global Change* **2010**, *15*, 703–719. doi:10.1007/s11027-010-9237-y.
22. Brown, S.; Nicholls, R.J.; Lowe, J.A.; Hinkel, J. Spatial variations of sea-level rise and impacts: An application of DIVA. *Climatic Change* **2016**, *134*, 403–416.
23. Juhász, L.; Podolcsák, A.; Doleschall, J. Open Source Web GIS Solutions in Disaster Management – with Special Emphasis on Inland Excess Water Modeling. *Journal of Environmental Geography* **2016**, *9*, 15–21. doi:10.1515/jengeo-2016-0003.
24. Ramanayake, K.; Vithanage, D.; Hettiarachchi, N.; Rathnayake, G.; Rajapaksha, S.; Fernando, N. Geo-enabled FOSS tool supports for immediate flood disaster response planning. 7th International Conference on Information and Automation for Sustainability, 2014, pp. 1–6. ISSN: 2151-1810, doi:10.1109/ICIAFS.2014.7069575.
25. Dutta, U.; Singh, Y.K.; Prabhu, T.S.M.; Yendargaye, G.; Kale, R.G.; Kumar, B.; Khare, M.; Yadav, R.; Khattar, R.; Samal, S.K. Flood Forecasting in Large River Basins Using FOSS Tool and HPC. *Water* **2021**, *13*, 3484. Number: 24 Publisher: Multidisciplinary Digital Publishing Institute, doi:10.3390/w13243484.
26. Lichter, M.; Felsenstein, D. Assessing the costs of sea-level rise and extreme flooding at the local level: A GIS-based approach. *Ocean & Coastal Management* **2012**, *59*, 47–62. doi:10.1016/j.ocecoaman.2011.12.020.

27. Li, X.; Grady, C.; Peterson, A.T. Delineating sea level rise inundation using a graph traversal algorithm. *Marine Geodesy* **2014**, *37*, 267–281. doi:10.1080/01490419.2014.902884.
28. Perini, L.; Calabrese, L.; Salerno, G.; Ciavola, P.; Armaroli, C. Evaluation of coastal vulnerability to flooding: comparison of two different methodologies adopted by the Emilia-Romagna region (Italy). *Natural Hazards and Earth System Sciences* **2016**, *16*, 181–194. doi:10.5194/nhess-16-181-2016.
29. NOAA. Detailed Method for Mapping Sea Level Rise Inundation. Method Description, NOAA Office for Coastal Management, 2017.
30. Styrin, E.; Luna-Reyes, L.F.; Harrison, T.M. Open data ecosystems: an international comparison. *Transforming Government: People, Process and Policy* **2017**, *11*, 132–156. doi:10.1108/TG-01-2017-0006.
31. Rajabifard, A.; Binns, A.; Masser, I.; Williamson, I. The role of sub-national government and the private sector in future spatial data infrastructures. *International Journal of Geographical Information Science* **2006**, *20*, 727–741. doi:10.1080/13658810500432224.
32. Goodchild, M.F.; Fu, P.; Rich, P. Sharing geographic information: an assessment of the Geospatial One-Stop. *Annals of the Association of American Geographers* **2007**, *97*, 250–266. doi:10.1111/j.1467-8306.2007.00534.x.
33. Folger, P. The Geospatial Data Act of 2018, 2018.
34. Choi, J.; Ahn, J.; Kim, H. A Cross National Comparison on the Awareness of Adopting FOSS4G to NSDI in Developing Countries. Free and Open Source Software for Geospatial (FOSS4G) Conference Proceedings, 2015, Vol. 15, p. 36. doi:10.7275/R5T43R86.
35. NOAA. A tutorial on datums. https://web.archive.org/web/20230512182749/https://vdatum.noaa.gov/docs/datums.html, 2023.
36. National Research Council. *Mapping the Zone: Improving Flood Map Accuracy*; National Academies Press: Washington, D.C., 2009. doi:10.17226/12573.
37. Gesch, D.B.; Gutierrez, B.T.; Gill, S.K. Coastal Elevations. In *Coastal Sensitivity to Sea-level Rise: A Focus on the Mid-Atlantic Region*; Titus, J.G.; Anderson, K.E.; Cahoon, D.R.; Gesch, D.B.; Gill, S.K.; Gutierrez, B.T.; Thieler, E.R.; Williams, S.J., Eds.; U.S. Climate Change Science Program: Washington, DC, USA, 2009; pp. 25–42.
38. NOAA. National Tidal Datum Epoch. https://web.archive.org/web/20230422174227/https://tidesandcurrents.noaa.gov/datum-updates/ntde/, 2023.
39. Juhász, L.; Hochmair, H.H.; de Santana, S.A.; Fu, Z.J. Sea Level Rise Impact Assessment Tool–A Web-Based Application for Community Resilience in Coral Gables, Florida. *International Journal of Spatial Data Infrastructures Research* **2020**, *15*, 36–55. doi:10.2902/1725-0463.2020.15.art2.
40. Danielson, J.J.; Poppenga, S.K.; Tyler, D.J.; Palaseanu-Lovejoy, M.; Gesch, D.B. Coastal National Elevation Database. USGS Fact Sheet 2018-3037, U.S. Geological Survey, 2018. doi:10.3133/fs20183037.
41. Harris, D.L. Tides and Tidal Datums in the United States. Technical Report SR-7, United States Army Corps of Engineers, Coastal Engineering Research Center, Fort Belvoir, VA, 1981.
42. Adhikari, S.; Ivins, E.R.; Frederikse, T.; Landerer, F.W.; Caron, L. Sea-level fingerprints emergent from GRACE mission data. *Earth System Science Data* **2019**, *11*, 629–646. Publisher: Copernicus GmbH, doi:10.5194/essd-11-629-2019.
43. Katsman, C.A.; Sterl, A.; Beersma, J.J.; van den Brink, H.W.; Church, J.A.; Hazeleger, W.; Kopp, R.E.; Kroon, D.; Kwadijk, J.; Lammersen, R.; Lowe, J.; Oppenheimer, M.; Plag, H.P.; Ridley, J.; von Storch, H.; Vaughan, D.G.; Vellinga, P.; Vermeersen, L.L.A.; van de Wal, R.S.W.; Weisse, R. Exploring high-end scenarios for local sea level rise to develop flood protection strategies for a low-lying delta—the Netherlands as an example. *Climatic Change* **2011**, *109*, 617–645. doi:10.1007/s10584-011-0037-5.
44. Shen, S.; Kim, K. Assessment of Transportation System Vulnerabilities to Tidal Flooding in Honolulu, Hawaii. *Transportation Research Record* **2020**, *2674*, 207–219. Publisher: SAGE Publications Inc, doi:10.1177/0361198120940680.
45. Parker, B.; Milbert, D.; Hess, K.; Gill, S. National VDatum–The implementation of a national vertical datum transformation database. Proceeding from the US Hydro'2003 Conference. Citeseer, 2003, pp. 24–27.
46. Paoa, N.; Fletcher, C.H.; Anderson, T.R.; Coffman, M.; Habel, S. Probabilistic sea level rise flood projections using a localized ocean reference surface. *Scientific Reports* **2023**, *13*, 2257. Number: 1 Publisher: Nature Publishing Group, doi:10.1038/s41598-023-29297-2.
47. SeaGIS. AusCoastVDT software version 1.20, Grid version 3.0 User Manual version 1.3, 2019.

48. Canadian Geodetic Survey. Vertical Datum Transformations. https://webapp.csrs-scrs.nrcan-rncan.gc.ca/geod/data-donnees/datum-transformation.php?locale=en, 2022.
49. NOAA. NOAA/NOS/CO-OPS Datums for Station 8723214, Virginia Key, Biscayne Bay FL. https://tidesandcurrents.noaa.gov/datums.html?id=8723214, 2023.
50. Zhang, K.; Dittmar, J.; Ross, M.; Bergh, C. Assessment of sea level rise impacts on human population and real property in the Florida Keys. *Climatic Change* **2011**, *107*, 129–146. doi:10.1007/s10584-011-0080-2.
51. Warmerdam, F. The geospatial data abstraction library. In *Open source approaches in spatial data handling*. *Advances in Geographic Information Science*; Hall.; Leahy., Eds.; Springer: Berlin, Heidelberg, 2008; Vol. 2, pp. 87–104. doi:10.1007/978-3-540-74831-1_5.
52. Neteler, M.; Bowman, M.H.; Landa, M.; Metz, M. GRASS GIS: A multi-purpose open source GIS. *Environmental Modelling & Software* **2012**, *31*, 124–130. doi:10.1016/j.envsoft.2011.11.014.
53. Flenniken, J.M.; Stuglik, S.; Iannone, B.V. Quantum GIS (QGIS): An introduction to a free alternative to more costly GIS platforms: FOR359/FR428, 2/2020. *EDIS* **2020**, *2020*. doi:10.32473/edis-fr428-2020.
54. Sweet, W.; Hamlington, B.; Kopp, R.; Weaver, C.; Barnard, P.; Bekaert, D.; Brooks, W.; Craghan, M.; Dusek, G.; Frederikse, T.; Garner, G.; Genz, A.; Krasting, J.; Larour, E.; Marcy, D.; Marra, J.; Obeysekera, J.; Osler, M.; Pendleton, M.; Roman, D.; Schmied, L.; Veatch, W.; White, K.; Zuzak, C. Global and Regional Sea Level Rise Scenarios for the United States: Updated Mean Projections and Extreme Water Level Probabilities Along U.S. Coastlines. NOAA Technical Report NOS 01, National Oceanic and Atmospheric Administration, National Ocean Service, Silver Spring, MD, 2022.
55. GPI Geospatial Inc.. Miami-Dade County LiDAR DEM. https://mdc.maps.arcgis.com/home/item.html?id=8c48d4bb8d9a42908f4936f698a2961a, 2021. Miami-Dade Open Data Hub.
56. Gill, S.K.; Schultz, J.R. Tidal datums and their applications. Report, NOAA, NOS Center for Operational Oceanographic Products and Services, 2001. doi:10.25607/OBP-170.
57. NOAA. Technical Considerations for Use of Geospatial Data in Sea Level Change Mapping and Assessment. NOAA Technical Report NOS 2010-1, 2010.
58. Marcy, D.; Brooks, W.; Draganov, K.; Hadley, B.; Haynes, C.; Herold, N.; McCombs, J.; Pendleton, M.; Ryan, S.; Schmid, K.; Sutherland, M.; Waters, K., New Mapping Tool and Techniques for Visualizing Sea Level Rise and Coastal Flooding Impacts. In *Solutions to Coastal Disasters 2011*; 2011; pp. 474–490. doi:10.1061/41185(417)42.